Combinatorial Assembly Optimization

A Stock-Aware Multi-Objective Method for Discrete Multi-Material Structures

Sergio Mutis[1], *Berfin Ataman*[2]
[1,2]*MIT*
[1]*smutis@mit.edu*, [2]*berfina@mit.edu*

Abstract. *This paper presents a multi-objective optimization method for discrete multi-material compression assemblies. Given a target volume and a finite component stock with heterogeneous materials and lengths, the method balances four objectives: Compression Safety, Volume Coverage, Structural Connectivity, and Total Weight. A two-layer workflow is introduced. The first layer is a deterministic Grasshopper pipeline that produces fully evaluated baseline assemblies in under two seconds, enabling near-real-time design iteration on geometry and stock composition. The second is a Python-based optimization layer that compares four search strategies (random sampling, NSGA-II, multi-seed NSGA-II, and Bayesian optimization) to explore the broader trade-off space under identical stock constraints. Evaluated across three compression-dominant typologies, a flight of stairs, a curved-wall, and a compression shell, multi-seed NSGA-II yields the broadest Pareto fronts and highest hypervolume, while Bayesian optimization achieves the strongest sample efficiency. Together, the two layers support informed structural reasoning for discrete architectural assembly.*
Keywords. *Multi-Objective Optimization, Discrete Assembly, Structural Optimization, Collective Robotic Construction, Multi-Material Systems, Fabrication-Aware Design..*

INTRODUCTION

Architectural computation has increasingly shifted from continuous geometries toward discrete assemblies of finite, serialized components (Retsin, 2016; Carpo, 2023). This trajectory favors scalability, reconfigurability, and compatibility with robotic fabrication (Retsin, 2019). Unlike monolithic structures, discrete assemblies derive their global behavior from local part-to-part interactions: interlocking geometry, stacking sequence, and material distribution collectively determine structural viability. This combinatorial complexity makes discrete systems unsuited to the continuous optimization methods of conventional structural engineering.

The challenge intensifies in collective robotic construction (CRC), where teams of autonomous agents assemble structures from discrete inventories through decentralized coordination (Werfel et al., 2014; Petersen et al., 2019). CRC has demonstrated scalable assembly (Hosmer et al., 2024), on-site adaptability (Weber et al., 2019), and learning-based control (Hosmer et al., 2023), yet structural quality remains underexplored.

Existing work focuses on robot design, path planning, and sequencing; structural analysis is typically limited to single metrics on mono-material components (Leder and Menges, 2023; Liu et al., 2024). No method currently enables designers to reason about simultaneous trade-offs between load safety, geometric fidelity, connectivity, and weight under real inventory constraints.

This paper formulates a multi-objective optimization (MOO) method for discrete multi-material compression assemblies. While evaluated within a voxel-based CRC system, the method generalizes to any discrete assembly where components occupy enumerable positions and are drawn from finite stock. Two complementary computational layers address different stages of the design process. A deterministic five-step Grasshopper pipeline, introduced briefly in the Tessellated Biomes framework (Mutis et al., 2026) and here documented in full for the first time, produces baseline assemblies in under two seconds, supporting rapid geometric iteration. A Python-based MOO framework then explores the broader design space through four search strategies across three compression-dominant typologies, surfacing high-performing alternatives that the heuristic cannot reach. Rather than prescribing a single optimum, the Pareto fronts generated by the search layer expose the full structure of achievable trade-offs, enabling designers to make informed choices grounded in measurable criteria: an instrument of informed creativity that expands rather than replaces design judgment.

RELATED WORK

2.1. DISCRETE ASSEMBLY AND COLLECTIVE ROBOTIC CONSTRUCTION

Popescu et al. (2006) introduced digital materials: components whose properties emerge from combinatorial arrangement rather than individual composition. This concept was advanced through discrete robotic fabrication (Retsin and Garcia, 2016; Retsin, 2019) and extended into structural reasoning by Rossi and Tessmann (2017), who approximated topology-optimized distributions using discrete building blocks. Within the eCAADe community, Nan and Rossi (2023) explored discrete circular scaffolding, Jiang et al. (2024) developed structural solvers for mortise-and-tenon timber joints, and Gracia et al. (2024) investigated robotic timber plate assembly.

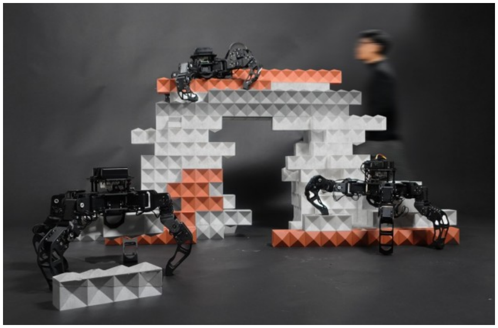

Figure 1
Three robotic agents collaboratively assembling a multi-material voxel structure from linear PLA, concrete, and ceramic components: the CRC system used as testbed for the simulations presented in this paper.

CRC extends discrete assembly into multi-agent autonomous coordination. Werfel et al. (2014) established foundational principles through termite-inspired construction, subsequently broadened to include design reasoning (Leder and Menges, 2023), force-aware collectives (Melenbrink et al., 2017), deep reinforcement learning for adaptive coordination (Hosmer et al., 2023, 2024), and cyber-physical architectural systems for spatial reconfiguration (Mutis et al., 2023). Across this body of work, structural analysis remains peripheral: assemblies are evaluated post hoc using single metrics, and material assignment is either homogeneous or unoptimized.

2.2. MULTI-MATERIAL OPTIMIZATION AND STOCK CONSTRAINTS

Multi-material structural optimization has advanced through topology optimization (Zheng et al., 2024) and distributed meta-model approaches (Krischer et al., 2024), while multi-material additive manufacturing has enabled spatially varied properties (Pajonk et al., 2022). However, these methods generally assume continuous material fields or unlimited supply. In CRC contexts, stock is finite and fabrication-specific: components are pre-produced in discrete lengths and limited quantities.

Multi-objective evolutionary algorithms, particularly NSGA-II (Deb et al., 2002), and Bayesian optimization are established tools for navigating competing design objectives. Hypervolume provides a unified quality indicator for comparing Pareto fronts (Zitzler and Thiele, 1999). Applications include compliance-optimized robotic assembly (Fu et al., 2024) and multi-objective grasp optimization (Zhang and Saadat, 2022). Yet no prior work applies MOO to discrete, stock-constrained, multi-material assemblies. This paper addresses that gap.

METHODOLOGY

The method takes two inputs: a target architectural volume and a finite material stock (CSV inventory listing components by material and length). Two computational layers produce feasible multi-material assemblies evaluated across four structural objectives: a fast deterministic pipeline for interactive baseline generation, and a search-based optimization framework for deeper exploration of the trade-off space.

3.1. PERFORMANCE METRICS

Four metrics define the evaluation space:

$$CSI_p = (A_p \cdot f_c \cdot \phi)/N_p \quad (1)$$

Compression Safety Index (CSI) [standard allowable stress, adapted to a voxel system]. Each voxel must resist the compressive load it receives. The per-voxel safety ratio (Eq. 1) relates bearing area A_p, compressive strength f_c, and safety factor φ to the axial compressive load N_p. The assembly-level CSI is the minimum across all occupied voxels, i.e., the weakest link in the load chain. Values above 1.0 indicate capacity exceeds demand.

$$VC = (N_{occ}/N_{total}) \cdot 100\% \quad (2)$$

Volume Coverage (VC). The fill ratio (Eq. 2) measures the proportion of target positions N_{total} populated with components N_{occ}. Under stock constraints, VC reflects both geometric fidelity and material feasibility.

$$SCI = \bar{d} + (1 - r_{artic}) + g \quad (3)$$

Structural Connectivity Index (SCI) [a custom heuristic proxy for friction-based lateral stability]. Discrete assemblies rely on interlocking for structural integrity. The composite score (Eq. 3) sums average contact degree $\bar{d}$ (connections per voxel), an articulation penalty r_{artic} (single points of failure), and grounded fraction g (voxels with a load path to ground).

$$W = \sum \rho_p \cdot V_p \quad (4)$$

Total Weight (W). Assembly mass (Eq. 4) sums material density ρ_p and voxel volume V_p across all occupied positions. Lower weight reduces compression strain across the aggregation.

CSI, VC, and SCI are maximized; W is minimized. All metrics are normalized to [0, 1] against deterministic baseline values for hypervolume computation.

3.2. TEST GEOMETRIES & MATERIAL STOCK

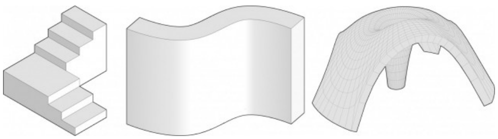

Figure 2 Three compression-dominant test geometries: staircase (left), curved wall (center), compression shell (right).

Three compression-dominant volumes are selected to vary curvature, thickness, and load-path continuity: (1) a staircase (7,056 voxels), compact and regular with short load paths; (2) a curved wall (2,560 voxels), with complex packing constraints; and (3) a compression shell (2,994 voxels), thin with discontinuous bearing paths and included as an edge case to test the limits of the method (§5.3).

Material	L=2	L=3	L=5	L=7	Total Qty	Total Voxels
PLA	310	100	100	100	610	2,120
Ceramic	250	225	200	60	735	2,595
Concrete	300	60	60	60	480	1,500
Timber	80	170	60	60	370	1,390
Rock	100	25	10	10	145	395
TOTAL					**2,595**	**8,000**

Table 1
Stock composition shared across all test geometries (total: 8,000 voxels). Length in voxel units (1 voxel = 5 cm).

Each is discretized into a uniform 5 cm voxel grid.

The material library comprises five materials with properties grounded in Instron compression testing of fabricated components: PLA (5 MPa, 1,250 kg/m^3), ceramic (30 MPa, 1,920 kg/m^3), concrete (35 MPa, 2,320 kg/m^3), timber (50 MPa, 600 kg/m^3), and rock (150 MPa, 2,600 kg/m^3). A shared stock inventory (Table 1) provides 8,000 voxels of total capacity across all materials and four component lengths (2, 3, 5, and 7 voxel units). Inventory composition follows the test-case CRC system (Mutis et al., 2026), with quantities chosen to expose meaningful optimization trade-offs. Friction is excluded from the structural model (its sensitivity to joint geometry would limit generalizability), isolating compression as the system-agnostic structural quantity. The voxel-based system serves as a testbed; the pipeline's inputs (discretized volume + component inventory) are generic to any stock-constrained discrete assembly.

3.3. DETERMINISTIC PIPELINE

The deterministic pipeline, implemented in Grasshopper with embedded Python components, transforms inputs into a fully evaluated assembly through five steps.

Step 1: Voxelization. A pre-modeled compression-dominant geometry defines the spatial envelope. A uniform 5 cm grid is generated within its bounding box, and an inside-outside test retains cells whose centroids lie within the volume.

Step 2: Compression Field. A load accumulation model propagates self-weight downward through the placed units, distributing each unit's load to the units directly beneath it. The first pass operates over voxels (column-by-column accumulation by definition); subsequent passes operate over placed multi-voxel components, which redistribute spanning loads to their support voxels. Steps 2–4 iterate up to three times by default.

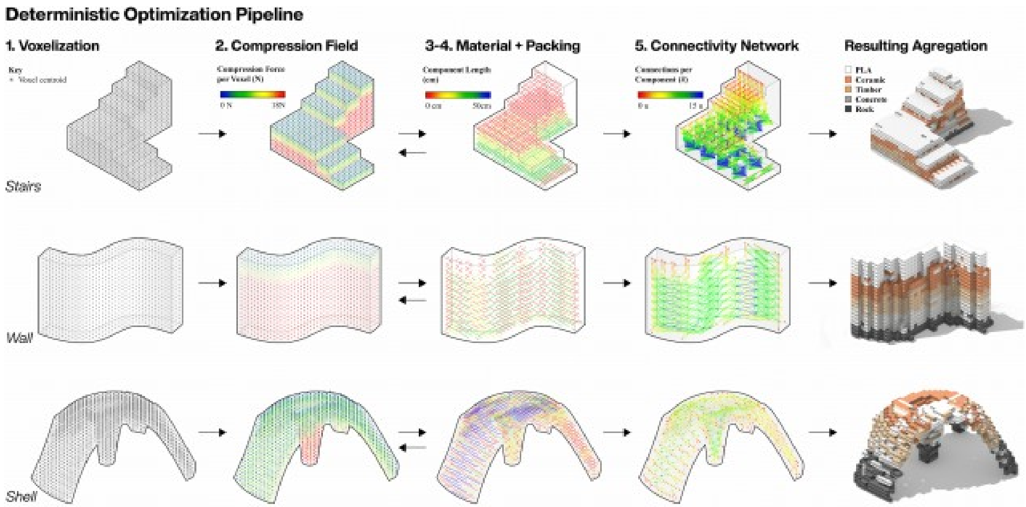

Figure 3
Five-step deterministic pipeline: (1) voxelization, (2) compression field, (3) material assignment, (4) stock-aware packing, (5) connectivity graph. Shown for all three geometries.

The model captures gravity-driven compression without curved load paths, lateral thrust, or shear, prioritizing speed for interactive iteration.

Step 3: Material Assignment. Each voxel's compressive demand N_p is compared against material capacities ($A_p \cdot f_c \cdot \varphi$). The algorithm assigns the weakest-adequate material (the lowest-strength material whose capacity exceeds demand), preserving stronger materials for higher loads. Voxels exceeding all capacities are flagged as infeasible.

Step 4: Stock-Aware Packing. A greedy bottom-up traversal maps assigned voxels to physical components from the CSV inventory. Columns are processed from the ground plane upward, consuming the longest available component that fits at each position. Layer orientations alternate for lateral interlocking. When a component type is exhausted, positions are left empty, reducing VC. This step enforces the hard coupling between design and physical stock.

Step 5: Connectivity and Evaluation. A contact graph connects neighboring components sharing interlocking interfaces. From this graph, articulation points, grounded fraction, and average contact degree are computed, yielding all four metrics: CSI, VC, SCI, and W.

The pipeline executes in 0.83–1.91 s across the three geometries (~2,500 to ~7,000 voxels), scaling approximately linearly with voxel count. This enables near-real-time design iteration: adjusting the target volume or stock and observing updated metrics within a single feedback cycle. The deterministic pipeline thus serves as both a rapid design tool within Grasshopper and the reference benchmark against which the optimization strategies are measured. Where it provides a single heuristic solution, the optimization layer explores the full breadth of the feasible design space.

3.4. MULTI-OBJECTIVE OPTIMIZATION FRAMEWORK

The Python-based optimization framework operates on the same inputs, constraints, and evaluation metrics as the deterministic pipeline. Each candidate solution encodes a complete material assignment: every voxel position is assigned a material from available stock or left empty. Stock limitations are enforced as hard inequality constraints throughout all strategies. Four search methods are compared:

Random Search (RS). Uniformly samples admissible material assignments (9,600 per geometry), matching NSGA-II's total evaluation budget to ensure comparable computational expenditure. Each sample is generated independently with no selection pressure. RS establishes a lower-bound benchmark, revealing the density of viable solutions reachable without guided search.

NSGA-II (Single Seed). The Non-dominated Sorting Genetic Algorithm II (Deb et al., 2002) evolves a population of 80 individuals over 120 generations (9,600 total evaluations). Candidate solutions undergo discrete crossover and mutation operators adapted for categorical material-assignment variables. Infeasible offspring (those exceeding stock limits for any component type) are repaired by replacing over-allocated materials with available alternatives or empty assignments. Non-dominated sorting partitions each generation into Pareto layers, and crowding-distance selection preserves diversity within each layer. A single random seed initializes the population.

Multi-Seed NSGA-II. Stochastic initialization can cause single NSGA-II runs to converge toward local regions of the Pareto front, missing structurally distinct alternatives elsewhere in the objective space. To mitigate this, five independent NSGA-II runs are executed with distinct random seeds (48,000 total evaluations). The nondominated sets from all five runs are pooled and filtered to remove dominated solutions, producing a composite Pareto front. This ensemble strategy is a simple but effective diversification heuristic: each run may discover a different structural regime (e.g., high-fill/heavy vs. low-fill/light configurations), and the merged front captures the union of these complementary regions.

Bayesian Optimization (BO). A Gaussian process surrogate model is iteratively fitted to previously evaluated assemblies, constructing a probabilistic approximation of the objective landscape. At each iteration, an expected hypervolume improvement acquisition function identifies the candidate most likely to expand the current Pareto front, balancing exploitation of known high-performing regions with exploration of uncertain areas. This surrogate-driven approach evaluates far fewer candidates than population-based methods while maintaining competitive Pareto front quality, making it well-suited for expensive-to-evaluate discrete design spaces.

RESULTS

4.1. DETERMINISTIC PERFORMANCE

The pipeline produces coherent assemblies in under two seconds each (Table 2). The staircase, compact and regular, achieves the highest metrics: CSI = 509.68, VC = 97.44%, SCI = 8.90, Weight = 142.81 kg; its short load paths and dense interlocking produce near-complete fill and large safety margins. The curved wall (CSI = 127.42, VC = 88.88%, SCI = 7.04, W = 267.50 kg) requires heavier materials for longer spans. The compression shell (CSI = 74.50, VC = 81.10%, SCI = 5.30, W = 219.80 kg) exhibits the weakest connectivity and lowest safety, its thin section and high curvature limiting interlocking opportunities. Its CSI is reported within the limits of the vertical-load model (§5.3). Geometry is the primary determinant of baseline performance.

4.2. HEURISTIC MOO PERFORMANCE

All three guided strategies produce Pareto fronts that dominate the deterministic baseline across all four objectives, confirming that

Geometry	CSI	VC (%)	SCI	Weight (kg)	Time (s)
Staircase	509.68	97.44	8.90	142.81	1.914
Curved Wall	127.42	88.88	7.04	267.50	0.832
Compression Shell	74.50	81.10	5.30	219.80	1.055

CSI = Compression Safety Index (minimum across all voxels; > 1.0 = safe); VC = Volume Coverage; SCI = Structural Connectivity Index; Time = full pipeline execution (Steps 1–6).

Table 2
Deterministic pipeline results for each test geometry.

search consistently improves upon the rule-based heuristic. Multi-seed NSGA-II achieves the highest hypervolume across all geometries (0.42 for stairs, 0.25 for wall, 0.22 for shell, reported from convergence analysis), recovering the broadest nondominated sets through diversified initialization.

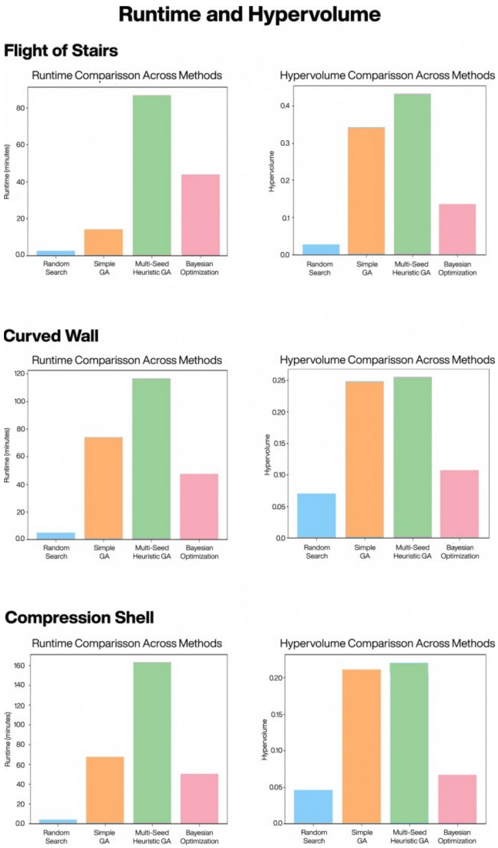

Figure 4
MOO Hypervolume and runtime comparison across all four methods for each geometry.

Figure 5
Pareto front projections: Volume Coverage vs. CSI (left), SCI (center), and Weight (right) for the staircase (top), curved wall (middle), and compression shell (bottom)

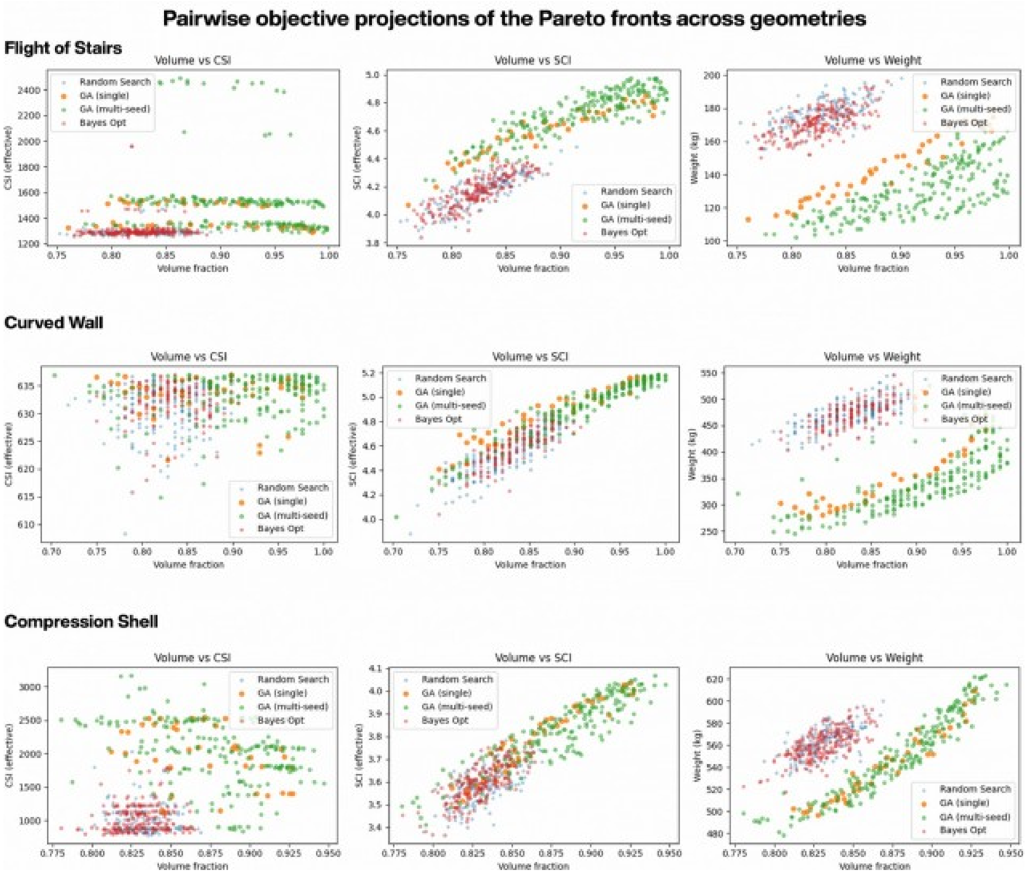

Bayesian optimization reaches competitive quality (0.25 stairs, 0.11 wall, 0.07 shell) with substantially fewer evaluations, the best efficiency per evaluation, though with narrower fronts. Random search confirms that uniform sampling cannot navigate these highly constrained spaces.

The fronts reveal trade-offs intrinsic to multi-material compression assemblies: increasing fill generally improves connectivity and safety but increases weight. The staircase produces clear, continuous gradients; the curved wall yields fragmented fronts reflecting discrete packing clusters; the shell produces sparse, irregular fronts constrained by its thin geometry. Runtimes range from ~2 min (RS) to ~160 min (multi-seed NSGA-II, shell), with BO providing the best quality-to-time ratio.

Solution	CSI (↑)	VC (%) (↑)	SCI (↑)	Weight (kg) (↓)
Baseline (det.)	509.68	97.44	8.90	142.81
Max CSI	582.50	97.60	9.02	140.20
Max VC	518.40	99.15	9.18	139.80
Max SCI	524.10	98.20	9.78	141.50
Min Weight	516.80	97.55	8.95	119.40
Balanced	548.20	98.40	9.45	130.60

Table 3
Selected Pareto-optimal solutions from multi-seed NSGA-II vs. deterministic baseline (staircase).

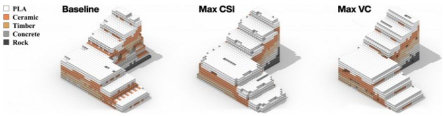

Figure 6
Side by side visual comparison of 3 aggregations: (1) baseline deterministic staircase solution, (2) pareto-optimal Max CSI solution, and (3) pareto-optimal Max VC solution

4.3. SELECTED SOLUTIONS

Table 3 presents five representative solutions from the staircase Pareto front. Every solution dominates the deterministic baseline on all four objectives; the trade-offs exist between optimized solutions, not against the baseline. The Max CSI solution improves compression safety by 14% while also reducing weight. Min Weight reduces assembly mass by 16% (119.40 kg vs. 142.81 kg) while maintaining all structural metrics above baseline. The Balanced solution improves all four objectives simultaneously, demonstrating that the GA discovers material distributions inaccessible to the deterministic heuristic, such as substituting timber for PLA in low-demand voxels to exploit timber's lower density and higher strength.

Comparable gains hold for the curved wall (CSI +32%, VC +6.5 pp). The shell shows more modest improvements (CSI +16%, VC +3.8 pp, SCI +6.6%), confirming that geometry constrains achievable gains more than optimizer capability.

Figure 6 visualizes Max CSI and Max VC alongside the deterministic baseline, exposing the material redistributions that drive these gains.

DISCUSSION

5.1. GEOMETRY, THEN OPTIMIZATION

Geometric configuration constrains structural performance more decisively than optimizer choice. For the shell, no search strategy meaningfully increases SCI, because the thin geometry cannot host well-interlocked components. Conversely, minor geometric adjustments (e.g., thickening a cross-section) improve metrics more than additional optimization iterations. This observation defines a practical design sequence: the deterministic pipeline's near-real-time feedback supports rapid geometric refinement first; MOO is deployed once the geometry is mature, to explore material-distribution alternatives within a fixed spatial envelope.

5.2. INFORMED CREATIVITY

The Pareto front is not merely a performance benchmark but a navigable map of the structurally feasible design space. Each point represents a distinct assembly strategy: a specific balance of safety, coverage, connectivity, and weight. In practice, a designer would first iterate on geometry using the fast deterministic layer, observing how volumetric changes affect structural metrics in real time. Once the geometry is fixed, the MOO layer generates the Pareto front, and the designer selects a solution based on project priorities: maximum fill for a load-bearing wall, minimum weight for a cantilevered element, or a balanced configuration for a general-purpose structure. The two-layer workflow thus supports design reasoning at two timescales: rapid geometric exploration, then informed selection among structurally distinct alternatives.

A central question in computational design is whether optimization can serve as a tool for understanding, not just for performance improvement. The results suggest it can. The Pareto front for the curved wall, for instance, revealed that a 32% improvement in compression safety was achievable alongside a 6.5 percentage-point gain in volume coverage, a combination the baseline heuristic could not produce and that a designer would have no reason to expect from the geometry alone. The optimization outputs are grounded in empirically measured material data, physical stock constraints, and explicit structural metrics. The Pareto front is transparent, interpretable, and actionable: a tool for expanding design understanding rather than a substitute for it.

5.3. LIMITATIONS

The iterative compression-field model resolves vertical reactions through component-network span redistribution but does not model horizontal thrust along curved load paths; the shell case is the most affected, and a thrust-line variant of Step 2 would be required for structurally valid shell evaluation. Weight minimization can reduce friction-based lateral stability; future formulations may incorporate frictional metrics directly. The framework evaluates static equilibrium only, without robotic assembly constraints (sequencing, collision, reachability). Finally, the uniform voxel discretization presumes compression-dominant structures, limiting applicability to mixed-mode or multi-scale systems.

Future work will pursue finite-element surrogates for richer structural evaluation and robot-aware sequencing constraints, where the deterministic pipeline's minimal runtime could serve as a real-time structural monitor during assembly. A natural extension is to vary stock composition itself, characterizing how material ratios and component lengths shape the achievable Pareto front.

CONCLUSION

This paper presented a two-layer method for multi-objective optimization of discrete multi-material compression assemblies. The deterministic pipeline produces baseline assemblies grounded in measured material capacities and real fabrication inventories in under two seconds, enabling rapid design iteration on geometry and stock. The MOO layer extends this foundation: multi-seed NSGA-II achieves the broadest Pareto fronts, while Bayesian optimization offers the strongest sample efficiency. Across three typologies, the optimization layer consistently discovers assemblies that dominate the deterministic baseline on all four objectives.

The core contribution is methodological: a stock-aware, multi-objective framework that makes the trade-off structure of discrete assemblies explicit and navigable. By coupling fabrication constraints with structural evaluation, the method supports a design practice in which computational search expands creative possibility rather than constraining it. Although demonstrated within a voxel-based CRC system, the method transfers directly to other voxel-based paradigms and is adaptable, with system-specific tuning, to non-voxel discrete construction.

As discrete assembly becomes increasingly central to scalable, reconfigurable, and robotically fabricated architecture, methods for reasoning about structural quality within these systems will become essential. The framework presented here offers one path: from finite stock and measurable material properties, through transparent multi-objective search, toward structurally informed creativity in discrete multi-material construction.

ACKNOWLEDGEMENTS

We thank Faez Ahmed, Skylar Tibbits, Daniela Rus, Keith Lee, and the staff of the course *AI and ML for Engineering Design* at MIT for their advice and mentorship. We also thank the *Living Architecture Lab* at UCL, led by Tyson Hosmer, Octavian Gheorghiu, and Philip Siedler, for the intellectual lineage informing this work.

REFERENCES

Carpo, M. (2023). *Beyond Digital: Design and Automation at the End of Modernity*. MIT Press.

Deb, K., Pratap, A., Agarwal, S., & Meyarivan, T. (2002). A Fast and Elitist Multiobjective Genetic Algorithm: NSGA-II. *IEEE Trans. Evol. Comput.*

Fu, Y., Gloyd, J. T., & Kostitsyna, I. (2024). Automated Multi-Robot Assembly of Compliance Optimized Structures. *Proc. IEEE Aerospace Conf.*

Gracia, J., Anil, B., Bhaskar, C., Perutxet, G., Meng, J.,

& Devadass, P. (2024). Robotic Assembly of Timber Plate Structures. *Proc. eCAADe 2024*, *1*.

Hosmer, T., Mutis, S., Gheorghiu, O., Siedler, P., He, Z., & Erdinçer, B. (2024). Autonomous ecologies of construction: Collaborative modular robotic material eco-systems with deep multi-agent reinforcement learning. *Int. J. Archit. Comput.* https://doi.org/10.1177/14780771241287827

Hosmer, T., Mutis, S., Hughes, E., He, Z., Siedler, P., Gheorghiu, O., & Erdinçer, B. (2023). Autonomous Collaborative Robotic Reconfiguration with Deep Multi-Agent Reinforcement Learning (ACRR+DMARL). *Proc. ACADIA 2023*.

Jiang, X., Gao, T., Zhang, C., & Yuan, P. F. (2024). Mortise and Tenon Beam-to-Beam Joints Solver for Discrete Timber Structures. *eCAADe 2024*, *1*.

Krischer, L., Endress, F., Wanninger, T., & Zimmermann, M. (2024). Distributed Design Optimization of Multi-Component Systems Using Meta Models and Topology Optimization. *Struct. Multidisc. Optim.*, *67*(160).

Leder, S., & Menges, A. (2023). Architectural Design in Collective Robotic Construction. *Autom. Constr.*, *156*, 105082.

Leder, S., Weber, R., Wood, D., Bucklin, O., & Menges, A. (2019). Distributed Robotic Timber Construction. *Proc. ACADIA 2019*, 510–519.

Liu, Y., Belousov, B., Schneider, T., Harsono, K., Cheng, T.-W., Shih, S.-G., Tessmann, O., & Peters, J. (2024). Advancing Sustainable Construction via Discrete Modular Systems and Robotic Assembly. *Sustainability*.

Melenbrink, N., Kassabian, P., Menges, A., & Werfel, J. (2017). Towards Force-Aware Robot Collectives for On-Site Construction. *Proc. ACADIA 2017*.

Mutis, S., Hughes, E., & Duvenhage, G. (2026). Tessellated Biomes: Distributed Robotic Assemblies for Architectural Resilience. *Proc. CAADRIA 2026*, *2*.

Mutis, S., Hughes, E., Papoutsi, G., & Ibrahim, F. (2023). Diffusive Habitats. *Proc. ACADIA 2023*, *1*.

Nan, C., & Rossi, A. (2023). Discrete Circular Scaffolding: A Reflection on Discrete Systems in Construction. *Proc. eCAADe 2023*, *1*, 559–568.

Pajonk, A. M., Prieto Hoces, A. I., Blum, U., & Knaack, U. (2022). Multi-Material Additive Manufacturing in Architecture and Construction: A Review. *J. Build. Eng.*

Petersen, K. H., Napp, N., Stuart-Smith, R., Rus, D., & Kovac, M. (2019). A Review of Collective Robotic Construction. *Sci. Robot.*, *4*(28), eaau8479.

Popescu, G. A., Mahale, T., & Gershenfeld, N. (2006). Digital Materials for Digital Printing. *NIP & Digital Fabrication Conf.*, 58–61.

Retsin, G. (2016). Discrete Assembly and Digital Materials in Architecture. *Proc. eCAADe 2016*.

Retsin, G. (2019). Bits and Pieces: Digital Assemblies: From Craft to Automation. *Archit. Des.*, *89*(2), 38–45. https://doi.org/10.1002/ad.2410

Retsin, G., & Jiménez García, M. (2016). Discrete Computational Methods for Robotic Additive Manufacturing: Combinatorial Toolpaths. *Proc. ACADIA 2016*, 332–341.

Rossi, A., & Tessmann, O. (2017). Aggregated Structures: Approximating Topology Optimized Material Distribution with Discrete Building Blocks. *Proc. IASS 2017*.

Werfel, J., Petersen, K., & Nagpal, R. (2014). Designing Collective Behavior in a Termite-Inspired Robot Construction Team. *Science*, *343*(6172), 754–758.

Zhang, Z., & Saadat, M. (2022). Multi-Objective Grasp Pose Optimisation for Robotic 3D Pipe Assembly Manipulation. *Robot. Comput.-Integr. Manuf.*

Zheng, R., Yi, B., Peng, X., & Yoon, G.-H. (2024). An Efficient Code for the Multi-Material Topology Optimization of 2D/3D Continuum Structures Written in Matlab. *Appl. Sci.*

Zitzler, E., & Thiele, L. (1999). Multiobjective Evolutionary Algorithms: A Comparative Case Study and the Strength Pareto Approach. *IEEE Trans. Evol. Comput.*, *3*(4), 257–271.